# Poynting flux evolution in Active Regions

Northumbria University NEWCASTLE

**André Chicrala & Shaun Bloomfield**

andre.silva@northumbria.ac.uk

GitHub

## Abstract

Evolution of solar active regions (ARs) is directly related to the occurrence of flares and coronal mass ejections. In this sense, changes in AR magnetic field can be used to unveil other relevant features like plasma flows in the region. Here, observations of surface 3D vector magnetic field from SDO/HMI are studied with the differential affine velocity estimator for vector magnetograms (DAVE4VM) to recover 3D plasma flows in the photosphere. The evolution of vertical Poynting flux (separated into components due to magnetic flux emergence and horizontal motions) is presented for different ARs that produce differing levels of flaring activity over the time they were observed.

## Introduction

Active Regions (ARs) are defined by their magnetic structure that can store large amounts of energy. Changes in the stored magnetic energy that may be released through large-scale reconnection are mainly caused by magnetic flux emergence, flux cancellation, and twisting of the field. In this work, 11 ARs are studied with the following objectives:

1. Observe the how the Poynting flux components accumulate over an AR structure;
2. Check the typical values obtained for the whole sample;
3. Compare the lifetime evolution of these region.

## Data and Methodology

Velocity fields in the photosphere can be estimated using sequences of magnetic field images through methods such as local correlation tracking (Leese 1970). Given the availability of Solar Dynamics Observatory (SDO) Helioseismic and Magnetic Imager (HMI) (Scherrer 2012) vectormagnetic observations, the use of the differential affine velocity estimator for vector magnetograms (DAVE4VM; Schuck 2008) is more appropriate. In this work we used a Python version of DAVE4VM.

For this work we use the Spaceweather HMI Active Region Patch (SHARP) series (`hmi.sharp_cea_720s`) that is provided at a cadence of 720 s (i.e., 12 minutes). In particular, the spherical magnetic field representation ($B_r$, $B_\phi$, $B_\theta$) is chosen, which has been remapped from plane-of-sky sampling into a Lambert Cylindrical Equal Area (CEA) projection.

After obtaining the 3D velocity components, these can be combined with the vectormagnetic field components to study the Poynting flux. Considering a plane $S$, the vertical component of the Poynting flux can be described as (Kusano 2002),

$$\dot{E} = \frac{1}{\mu_0}\int_S \mathbf{B}\times(\mathbf{v}\times\mathbf{B})\cdot\mathbf{n}dS = \dot{E}_t + \dot{E}_n\,, \tag{1}$$

that can be split into the component due to tangential (i.e., horizontal) motions and flux emergence,

$$\dot{E}_t = -\frac{1}{\mu_0}\int_S (\mathbf{v}_t\cdot\mathbf{B}_t)\,\mathbf{B}_n\cdot\mathbf{n}dS\,, \qquad \dot{E}_n = \frac{1}{\mu_0}\int_S B_t^2\mathbf{v}_n\cdot\mathbf{n}dS\,. \tag{2}$$

In implementing the above equations, the tangential field $\mathbf{B}_t = (B_\phi, -B_\theta, 0)$ is the combination of the longitudinal and latitudinal components of the spherical magnetic field, while the normal field $\mathbf{B}_n = (0, 0, B_r)$ contains only the radial component. Using the velocities obtained by PyDAVE4VM the normal, tangential, and total vertical Poynting flux are then calculated considering integration over the pixel surface area.

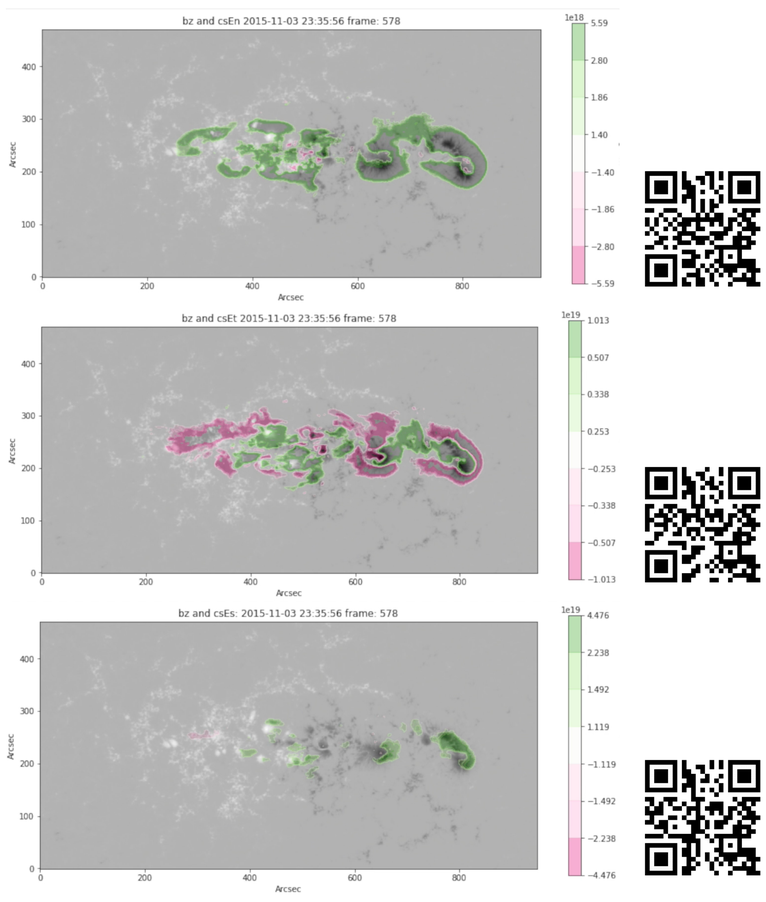


**Figure 1:** Cumulative pixel integrated Poynting flux ($\dot{E}_s$, $\dot{E}_n$, $\dot{E}_t$) for NOAA 12443. In the videos the filled contours were drawn at the 5% largest values for this AR energy flux which range from $10^{16}$ to $10^{18}$ Watts. The QR codes can be used to access the videos.

## Results

Looking at the individual values for each pixel of the Poynting flux components images, in a set that has 13590 individual entries for 11 different ARs, it is possible to observe from histograms that the total Poynting flux $E_s$ is consistent with what was reported in the literature. In addition to that the typical values for the Poynting flux typical components are shown.

The videos for the ARs are so far showing that the Poynting flux tend to build up around the spots. Sample videos showing the Poynting flux ($\dot{E}_s$, $\dot{E}_n$, $\dot{E}_t$) cumulative sum for NOAA 12443 can be accessed using the QR codes in Figure 1.

The values contained in each of the images of the vertical Poynting flux components were then integrated over the entire AR field-of-view to investigate the net energy flux through the photosphere for each individual component of an AR (Figure 2).

**Table 1:** ARs currently registered in the results database.

| HARP No. | NOAA No. | Observation Dates First | Observation Dates Last | Sample Size | Hale class evolution sequence |
|---|---|---|---|---|---|
| 2585 | 11705 | 2013-03-21 | 2013-04-02 | 1302 | $\beta$, $\alpha$, plage |
| 2587 | 11704 | 2013-03-23 | 2013-04-03 | 1266 | $\alpha$, $\beta$, $\alpha$, $\beta$, $\alpha$, $\beta$ |
| 2887 | 11778 | 2013-06-24 | 2013-07-04 | 1240 | $\alpha$, $\beta$, $\beta\gamma$, $\beta$ |
| 3686 | 11967 | 2014-01-30 | 2014-02-08 | 1015 | $\beta$, $\beta\gamma$, $\beta\gamma\delta$ |
| 4448 | 12139 | 2014-08-11 | 2014-08-23 | 1368 | $\beta$, $\beta\gamma$, $\beta$ |
| 5011 | 12253 | 2014-12-30 | 2015-01-10 | 1291 | $\beta$, $\beta\gamma$, $\beta\gamma\delta$, $\beta\gamma$, $\beta$, $\alpha$ |
| 5026 | 12257 | 2015-01-04 | 2015-01-13 | 1107 | $\beta$, $\beta\delta$, $\beta\gamma\delta$, $\beta\gamma$ |
| 6063 | 12443 | 2015-10-30 | 2015-11-09 | 1266 | $\beta$, $\beta\gamma\delta$, $\beta\gamma$, $\beta\delta$, $\beta$, $\alpha$ |
| 6223 | 12477 | 2016-01-02 | 2016-01-12 | 1212 | $\alpha$, plage |
| 6558 | 12546 | 2016-05-15 | 2016-05-26 | 1316 | $\alpha$, $\beta$, $\alpha$ |
| 6846 | 12611 | 2016-11-16 | 2016-11-26 | 1207 | $\alpha$, $\beta$, $\alpha$, plage |

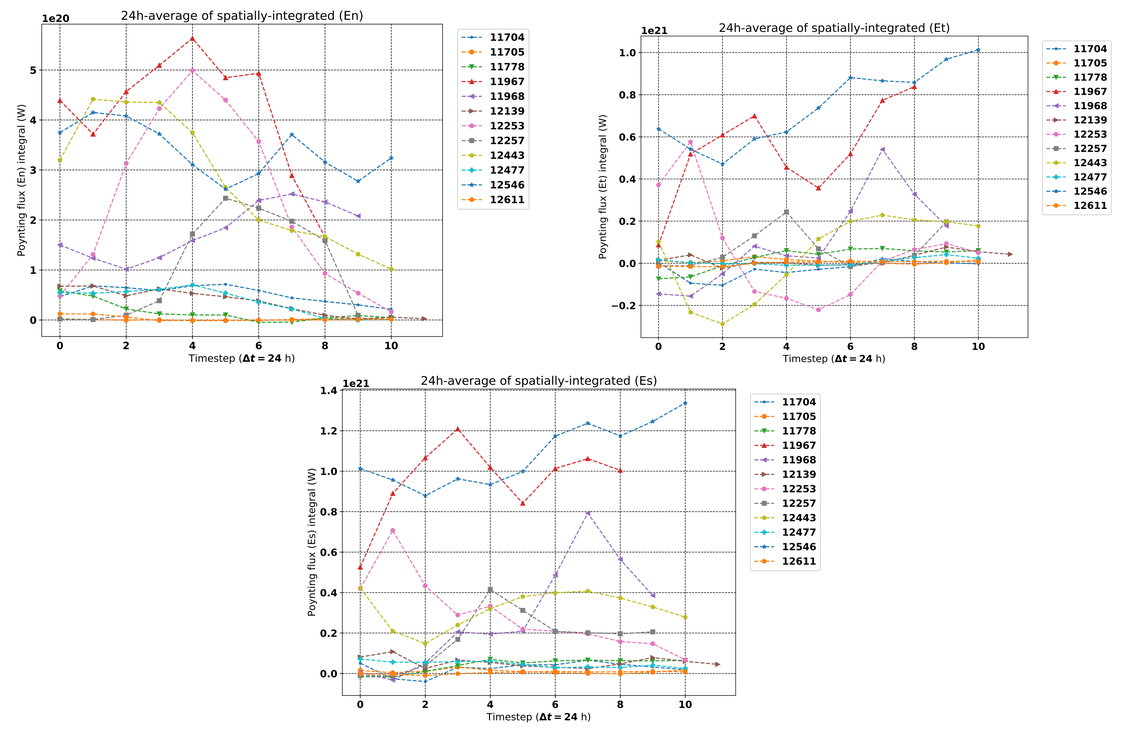


**Figure 2:** Daily average for the integrated Poynting flux values of each AR.

## Conclusions

- For the entire data set 70 to 80% of the Spatially integrated Poynting flux absolute values range from $10^{13}$ to $10^{14}$W (which corresponds to $10^5$ to $10^7$ erg cm$^{-2}$ s$^{-1}$).
- As the analysis is getting carried on the largest values of the Spatially integrated Poynting flux ($10^{16}$ to $10^{18}$W) are consistently being found around the spots of the ARs.
- ARs with a more complex structure tend to present larger values for Poynting flux;
- The data also suggests that the evolution of both the spatially integrated Poynting flux and Hale class are somehow linked.

## Forthcoming Research

It is intended to search for spatially-resolved characteristics in the energy injection components that may be related to flaring activity. That will require the addition of two new tables to the database with information about the ARs morphology and energetic events. The analysis of velocity flows and energy injection rates will then be repeated over many additional ARs with different levels of flaring activity and magnetic complexity, allowing a statistical study of how these energy-related parameters impact the evolution of ARs and their relation to flaring.

## References

Kusano, K., et al. 2002, *ApJ*, **577**, 501

Leese, et al. 1970, *Pattern Recognition*, **2**, 279

Scherrer, P.H., et al., 2012, *Sol. Phys.*, **275**, 207

Schuck, P.W., 2008, *ApJ*, **683**, 1134

## Acknowledgements

AC gratefully acknowledges funding in the form of a Northumbria University RDF Studentship. Data are provided courtesy of NASA/SDO and the HMI science team.

## Poster file